Variation of the meiotic recombination landscape and properties over a broad evolutionary distance in yeasts

Christian Brion[1], Sylvain Legrand[2], Jackson Peter[1], Claudia Caradec[1], David Pflieger[1], Jing Hou[1], Anne Friedrich[1], Bertrand Llorente[2]*, Joseph Schacherer[1]*

1 Université de Strasbourg, CNRS, GMGM UMR 7156, Strasbourg, France, **2** CNRS UMR7258, INSERM U1068, Aix Marseille Université UM105, Institut Paoli-Calmettes, CRCM, Marseille, France

* schacherer@unistra.fr (JS); bertrand.llorente@inserm.fr (BL)

Abstract

Meiotic recombination is a major factor of genome evolution, deeply characterized in only a few model species, notably the yeast *Saccharomyces cerevisiae*. Consequently, little is known about variations of its properties across species. In this respect, we explored the recombination landscape of *Lachancea kluyveri*, a protoploid yeast species that diverged from the *Saccharomyces* genus more than 100 million years ago and we found striking differences with *S. cerevisiae*. These variations include a lower recombination rate, a higher frequency of chromosomes segregating without any crossover and the absence of recombination on the chromosome arm containing the sex locus. In addition, although well conserved within the *Saccharomyces* clade, the *S. cerevisiae* recombination hotspots are not conserved over a broader evolutionary distance. Finally and strikingly, we found evidence of frequent reversal of commitment to meiosis, resulting in return to mitotic growth after allele shuffling. Identification of this major but underestimated evolutionary phenomenon illustrates the relevance of exploring non-model species.

Author summary

Meiotic recombination promotes accurate chromosome segregation and genetic diversity. To date, the mechanisms and rules lying behind recombination were dissected using model organisms such as the budding yeast *Saccharomyces cerevisiae*. To assess the conservation and variation of this process over a broad evolutionary distance, we explored the meiotic recombination landscape in *Lachancea kluyveri*, a budding yeast species that diverged from *S. cerevisiae* more than 100 million years ago. The meiotic recombination map we generated revealed that the meiotic recombination landscape and properties significantly vary across distantly related yeast species, raising the yet to confirm possibility that recombination hotspots conservation across yeast species depends on synteny conservation. Finally, the frequent meiotic reversions we observed led us to re-evaluate their evolutionary importance.

Introduction

Accurate chromosome segregation at the first meiotic division often requires crossovers (COs) between homologous chromosomes [1]. Meiotic COs result from the repair of programmed DNA double strand breaks (DSBs) by homologous recombination, that can yield gene conversions through non reciprocal transfer of genetic variations (GCs) [2]. Only a fraction of DSBs yields CO-associated GCs, the remaining yielding GCs without associated COs, called non-crossovers (NCOs). Overall, meiotic recombination provides a large source of genetic diversity by rearranging allelic combinations and therefore plays a key role in evolution.

The budding yeast *S. cerevisiae* has long been a model to dissect recombination mechanisms. Meiotic recombination is initiated by Spo11-catalyzed DSBs [3] within nucleosome depleted regions enriched in gene promoters [4] in the context of chromatin loops organized around the synaptonemal complex [5]. Meiotic DSBs and COs occur within well-characterized hotspots across the genome. The mapping of 4,163 COs and 2,126 NCOs from 46 *S. cerevisiae* tetrads [6] showed that the frequency of meiotic recombination events correlates with previously localized DSBs [7,8]. It was also highlighted that the frequency of segregating chromosome without a CO is low in *S. cerevisiae* (1 out of 46 tetrads), supporting the importance of at least one CO per chromosome for accurate segregation [9,10,11].

Meiotic DSBs and associated recombination hotspots, driven by a sequence determinant, have long been expected to be extremely unstable across evolution because of their supposed inherent self-destructive nature [12]. Indeed, being preferentially cut, the strongest hotspots are expected to be preferentially converted with the weakest ones. This is the case in some mammalian species where DSB hotspots are determined by the sequence specific DNA binding of the fast evolving PRDM9 methyl transferase protein [13]. Remarkably, meiotic recombination initiation hotspots show a good conservation within *Saccharomyces* species despite a sequence divergence almost 10-fold higher than between human and chimpanzees that completely lack hotspot conservation [14–17]. The same observation was made for two *Schizosaccharomyces* species [18]. This likely results from the fact that DSB hotspots in yeasts lie in gene promoters, which are conserved functional elements and do not depend on sequence specific elements [15,19]. However, the *Saccharomyces* species have almost completely collinear genomes, which could favor hotspot conservation.

Here, we assessed the properties and variations of the meiotic recombination landscape by taking advantage of the broad evolutionary range of the Saccharomycotina species [20]. We explored the recombination landscape of the *Lachancea kluyveri* yeast species (formerly *Saccharomyces kluyveri*) that shares the same life cycle as *S. cerevisiae* but is a distantly related species, which diverged from it prior to a whole-genome duplication event for more than ~100 million years (*i.e.* protoploid species) [21,22].

Results and discussion

L. kuyveri meiotic recombination map reveals a high frequency of 4:0 segregating regions

To explore the *L. kluyveri* meiotic recombination landscape genome-wide we generated a diploid hybrid by mating two polymorphic haploid isolates, NBRC10955 (*MAT*a) and 67–588 (*MAT*α) [23]. The NBRC10955/67-588 hybrid contains approximately 85,705 polymorphic sites distributed across the eight homologous chromosomes, resulting in a genetic divergence of ~0.7% (S1 Fig). It sporulates efficiently, with a spore viability of 73% (S1 Fig). Overall, the divergence is in the same order of magnitude to those of the S288c/SK1 and S288c/YJM789 hybrids used for meiotic tetrad analysis in *S. cerevisiae* [6,24].

By whole genome sequencing, we genotyped all four viable spores from 49 meioses of the NBRC10955/67-588 hybrid. We selected a set of 56,612 reliable SNPs as genetic markers to define the allelic origin along the chromosomes (see material and methods and S2 and S3A Figs). This resulted in a median distance of 196 bp between consecutive markers, with only 27 inter-marker distances higher than 5 kb. These markers are well distributed across the genome, with the exception of the rDNA array on chromosome H and the subtelomeric regions. Subtelomeric regions carried low quality sequences and translocation events, which were manually determined. To avoid spurious identification of recombination events at the ends of the chromosomes, we disregarded some subtelomeric regions, adapting case by case their size according to the presence of translocations and/or to the poor sequence quality (S4 Fig). Altogether these regions range from 2 to 32 kb in size and represent 2% of the entire genome (251 kb).

From these data, we performed a detailed analysis of individual recombination events using the CrossOver program [25]. Across the 49 meioses, we identified 274 NCOs and 875 single COs (Fig 1A and S1 Table), 541 of which were associated with a detectable GC tract. Small GC tracks associated or not to COs might not overlap with enough genetic markers and the corresponding number could be underestimated. Surprisingly, we observed a high frequency of double COs, which correspond to two COs at the same location involving the four chromatids (138 events, 16% of the total COs) (Fig 1A) as well as a high frequency of regions with a 4:0 allelic segregation (505 regions) (Fig 1A). Previous *S. cerevisiae* studies reported mostly single COs and GC tracts with 3:1 allelic segregation [6,24,25]. These types of events involving the four chromatids simultaneously are usually expected to reflect mitotic recombination events preceding meiotic entry and are generally disregarded [6,24]. In our case, their quantitative importance prompted us to examine them more carefully.

High meiotic reversion frequency leads to extensive LOH events in meiotic products

We identified a total of 505 regions with a 4:0 segregation. The size distribution of these tracts follows a bimodal pattern with an almost equal partitioning of events in both clusters (Fig 1B). Based on this distribution, we defined two categories: short 4:0 regions (median = 2.3 kb, N = 213) and large 4:0 regions (median = 224 kb, N = 292) with a size cut-off of 10 kb (Fig 1B). The size distributions of the 213 short tracts smaller than 10 kb associated with COs and NCOs mimic the size distributions of the 3:1 conversion tracts associated with COs and NCOs (Fig 1C). The 292 large regions with a 4:0 segregation bear all the characteristics for being the results of mitotic G2 COs prior entry into meiosis that lead to large regions of loss of heterozygosity (LOH), ranging from 11 to 1,882 kb.

These 4:0 segregating regions and the double COs were found within 38 tetrads. In these tetrads, the number of large 4:0 regions varies between 2 to 18 and their cumulative size ranges from 5% to 63% of the genome (Fig 2A and 2B). All these large LOH regions are unique to each tetrad and the conserved allelic version seems random leading to an equal frequency of each parental allele (Fig 2B). However, these large LOH events are not equally distributed along the genome. Centromere-proximal regions show a very low rate of LOH events. Every chromosome carries LOH events with the exception of the 1-Mb introgressed region (Sakl0C-left) carrying the *MAT* locus that displays a systematic 2:2 segregation (Fig 2).

Overall, the frequency and repartition of 4:0 segregating regions and double COs support a high proportion of mitotic events prior meiotic entry. Such a mitotic genomic instability is unexpected, except from some mutants of genes involved in genome integrity maintenance for instance. To test the mitotic stability of the NBRC10955/67-588 hybrid, we induced an
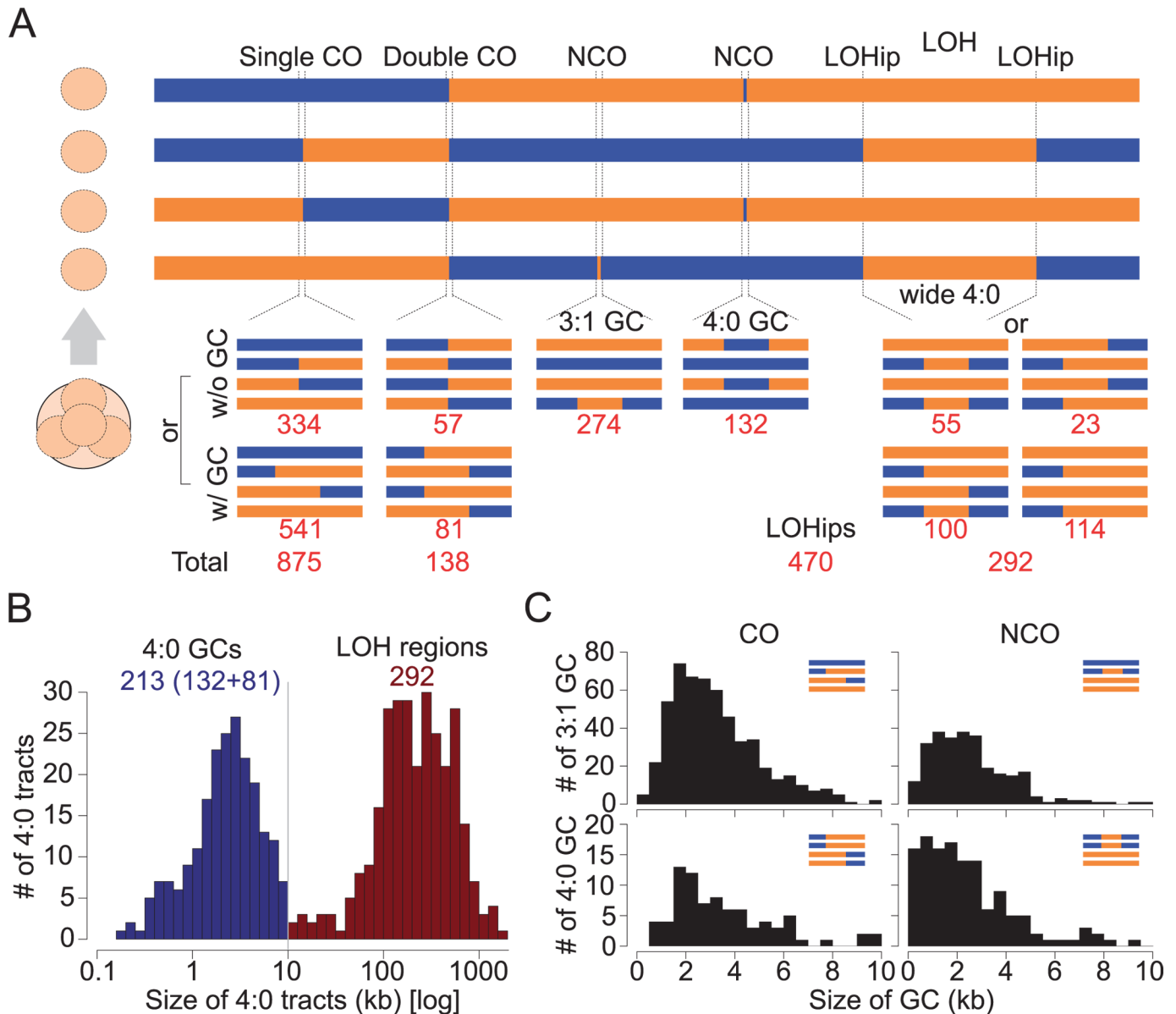
Fig 1. *L. kluyveri* recombination events classes. (A) Allelic segregation patterns observed within a four-spore viable tetrad. CO: crossover, NCO: non-crossover, GC: gene conversion, LOH: loss of heterozygosity, LOHip: LOH initiation point. Red values correspond to the number of instances detected across the 49 tetrads studied. (B) The 4:0 tracts were distinguished according to their sizes. The threshold of 10 kb was defined using the end of the peak corresponding to the short 4:0 tracts that are thought to result from meiotic 3:1 GCs after RTG. (C) Comparison of the distribution of GCs sizes. Top left: 3:1 GCs associated to COs. The median size is 2.8 kb. Bottom left: 4:0 GCs associated to COs. The median size is 3.0 kb. Top right 3:1 GCs associated to NCOs. The median size is 2.3 kb. Bottom right: 4:0 GCs associated to NCOs. The median size is 1.9 kb.

accumulation of mitoses by generating two independent mutation accumulation lines. They went through 12 single cell bottlenecks on rich medium representing ~ 240 generations. The sequence analysis of the two evolved diploids as well as the initial parental diploid (only ~ 40 generations) revealed no LOH event (S5 Fig). In conclusion, the frequency of mitotic recombination on rich medium of the NBRC10955/67-588 hybrid is too low to explain the high amount of LOH events in the dissected tetrads, and therefore that these events most likely occurred during meiosis.
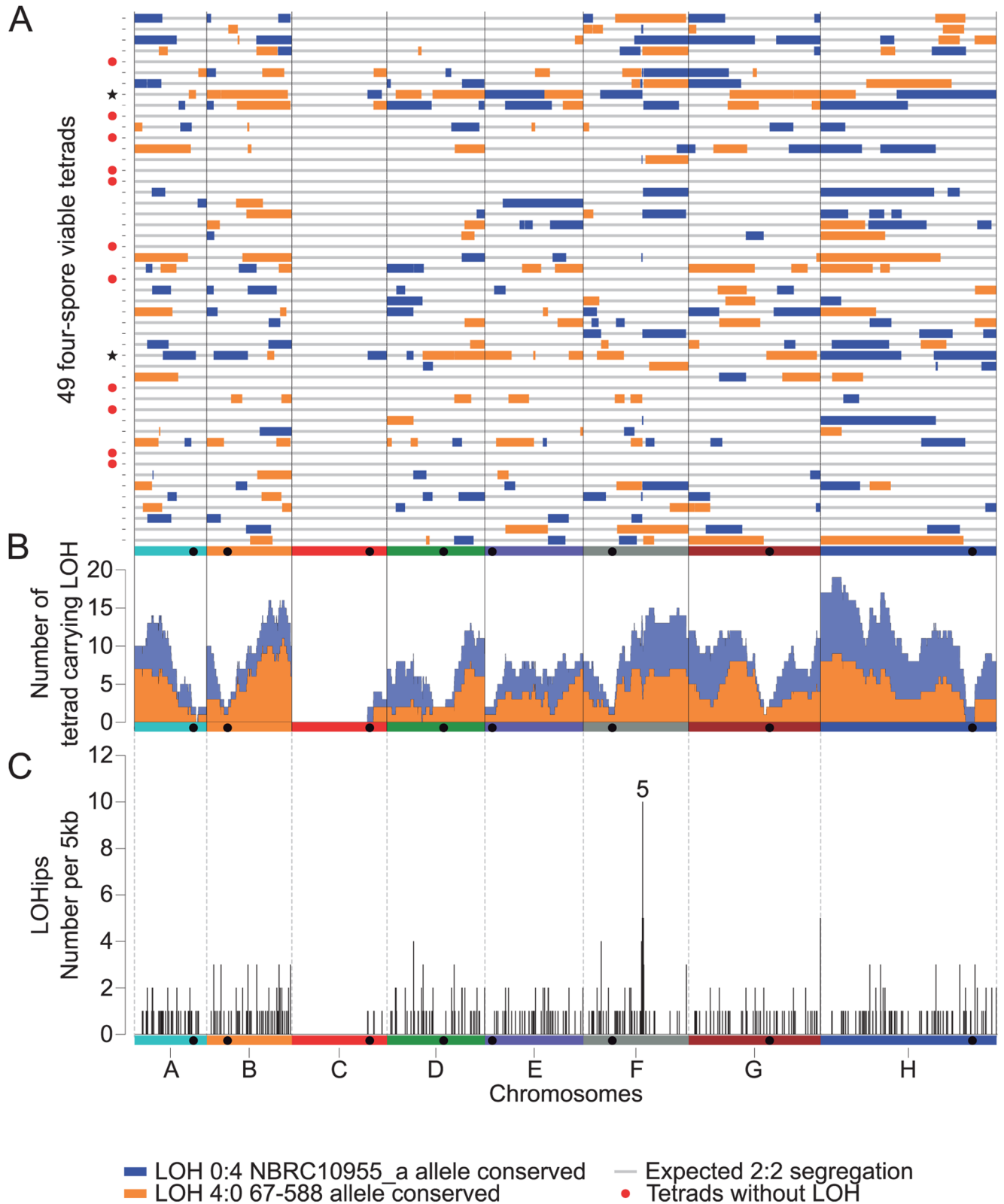
Fig 2. Distribution of LOH events across the 49 sequenced tetrads. (A) Location of the LOH regions along the genome for each tetrad. Colors correspond to the allelic version conserved. Tetrads flagged by a red dot do not carry any LOH. The two tetrads flagged by a black star have all their centromeres included in LOH regions. (B) Frequency of LOH events along the genome across the 49 tetrads using a 5kb sliding

window. The frequency of LOH conserving NBRC10955 alleles (blue area) is added to the frequency of LOH conserving 67–588 alleles (orange area) to provide the total frequency of LOH events along the genome. (C) Frequency of LOHips along the genome using a 5 kb window. Region 5 is a hotspot of LOHips and overlaps with the *VMA1* gene. A total of 470 LOHips were detected across the 38 tetrads with LOH.

The only alternative explanation left is that the high frequencies of observed LOH, double CO and 4:0 GC events are due to the so-called "return to mitotic growth" (RTG), alternatives such as very active meiotic recombination hotspots but with peculiar recombination properties being unlikely. RTG is a meiotic reversion where cells enter into meiotic prophase, initiate inter-homolog meiotic recombination, but return to vegetative growth before meiosis I [26,27]. The reshuffled diploid obtained post RTG will go through a second meiosis resulting to the studied tetrad (Fig 3). The recombination events induced by the abortive meiosis occurring before the RTG are indistinguishable from inter-homolog mitotic G2 events (Fig 3). In support of a meiotic origin, we found a lack of LOH events near the centromeres, similar to canonical meiotic recombination events. However, two out of the 38 tetrads display LOH regions including all of the eight centromeres. A possible explanation for these two cases would be that RTG occurred after meiotic anaphase I. Such events would have escaped the meiotic commitment thought to be irreversible after meiotic prophase in *S. cerevisiae* through a positive feedback expression of the Ndt80 meiotic transcription factor [28].

Finally, RTG implies at least some residual growth on sporulation medium. We therefore isolated individual NBRC10955/67-588 hybrid cells on sporulation medium, and after two days, we did observe small colonies of about 0.5 mm of diameter, corresponding approximately to ten generations. This indicates that potassium acetate used as sporulation medium and cellular nutrients storage are enough to ensure residual growth, before starting sporulation. A possible explanation is that potassium acetate does not induce a strong enough starvation stress, due to the more respiratory lifestyle of this species [29,30].

Since RTG was highlighted, it has been suspected to happen in natural conditions and induce phenotypic diversity by generating new allelic combinations [31]. The ease with which *L. kluyveri* undergoes RTG leads us to consider that its frequency in natural conditions is high. The resulting LOH regions allow the expression of recessive alleles and new combination of interactive alleles. A recent study also demonstrated that COs induced during RTG can be used to generate an allelic reshuffled population allowing genetic linkage analysis [31]. Interestingly, RTG is initiated in stress conditions and the resulting allelic shuffling might increase the fitness to environment, immediately assuring cell survival. Therefore, the fact that RTG is easily induced in some yeast species can reveal a new mechanism of adaptation to stress, the generality of which remains to be determined.

VMA1 corresponds to a meiotic hotspot for double COs and LOHs

Our recombination map revealed that the main hotspot associated with RTG events, *i.e.* double COs, 4:0 NCOs and LOH regions corresponds to the *VMA1* gene located on chromosome F (hotspot 5, Fig 2C and S6 Fig). This gene encodes a subunit of a vacuolar ATPase and the PI-Sce1 endonuclease (also called Vde1) in *S. cerevisiae* as well as in *L. kluyveri* [32,33]. This is a site-specific endonuclease active during meiosis that promotes a homing reaction (S7 Fig). In a heterozygous diploid where only one of the *VMA1* alleles carries PI-Sce1, the endonuclease cleaves the *VMA1* sequence lacking the endonuclease-coding portion to initiate homing, which consists of a recombination reaction associated or not with a CO (S7 Fig). Using *de novo* genome assembly, we defined which version of *VMA1* was carried by each parental strain as well as in the other 26 *L. kluyveri* natural genomes already sequenced [23]. In total, nine strains harbor a *VMA1* gene with PI- Sce1, including our parental strain NRBC10955, and

nineteen isolates harbor an empty *VMA1* gene, including the other parental strain 67–588. Therefore, meiosis specific homing of PI-Sce1 explains the high recombinogenic activity at the *VMA1* locus observed in our dataset that includes five COs, five double COs, nine short 4:0 NCOs and ten LOH events (S6 Fig). Note that in a single meiosis, PI-Sce1 can cut one or two chromatids generating 3:1 and 4:0 NCOs as well as single and double COs, respectively. Therefore, in this specific case, only borders of long tracts of LOH can be unambiguously attributed to RTG events.

L. kluyveri has a lower recombination rate than *S. cerevisiae*

To estimate the number of recombination events per meiosis in *L. kluyveri*, we excluded double COs, 4:0 NCOs and large LOHs that are considered to result from RTG events. This results in 334 COs without detected GC, 541 single COs with 3:1 GC tracts and 274 NCOs in 49 meioses (Fig 1 and S1 Table). We also estimated that at least 100 single COs occurred within LOH regions (see below). This corresponds to 19.9 COs and 5.6 NCOs per meiosis on average. RTG events comprise 138 double COs, 178 large LOH tracts within chromosomes (100 + 55 + 23, Fig 1), 114 large LOH tracts encompassing one telomere and 132 4:0 NCOs. Each double CO corresponds to one CO per RTG. Large internal LOH tracts account for two COs per RTG. Telomere proximal LOH tracts account for one CO per RTG. Altogether, we observed 608 COs (138 double COs + 470 LOHips, Fig 1) and 132 NCOs from RTG within 38 meioses, corresponding to 16 COs and 3.5 NCOs per RTG on average considering that only one RTG occurred.

The detected recombination events per RTG correspond to an underestimation of the actual number of events since we analyzed only one of the two daughter cells after RTG (Fig 3). Considering that not all of the recombination events occurring during RTG are detected (as describe in [31]), we estimate that the average number of COs per RTG is similar to those per meiosis (S8 Fig).

The presence of LOH regions also leads to an underestimation of meiotic recombination events that occur in such regions. Even numbers of COs within a LOH region involving only two chromosomes are missed as well as all NCOs. Considering the global recombination rate, we estimate that about 190 COs are expected within LOH regions, 90 of which being not undetectable (see Methods).

Both COs and NCOs are significantly less abundant than in *S. cerevisiae* that has a similar genome size, and where 73 to 90 COs and 27 to 46 NCOs have been detected per meiosis, depending on the studied hybrid [6,24]. We used a stringent threshold for the detection of conversions (see Methods). This may have led us to miss some short conversions. Indeed, the median size of *L. kluyveri* conversion tracts is 2.9 kb for those associated with COs, and 2.2 kb for NCO conversion tracts (Fig 1B) compared to 2 kb and 1.8 kb in *S. cerevisiae*, respectively [6]. However, our strategy should reveal virtually all COs. Therefore, we can conclude that the genetic map of the *L. kluyveri* hybrid used is three to four times smaller than that of *S. cerevisiae*.

As previously observed in *S. cerevisiae* and in other species, the average number of COs per chromosome is correlated to chromosome length in *L. kluyveri*. Remarkably, the linear relation between chromosome size and number of COs displays a positive intercept of 1.0 CO for a virtual chromosome size of 0 bp both in *S. cerevisiae* and *L. kluyveri* (Fig 4A). This suggests that in these species the meiotic program is set up in such a way that at least one CO will form per chromosome independently of its length.

S. cerevisiae and *L. kluyveri* have a similar genome size of approximately 12 Mb and therefore the recombination rate is estimated to ~1.6 COs/Mb and ~6 COs/Mb for *L. kluyveri* and *S. cerevisiae*, respectively. This difference underlines the particularly high recombination rate
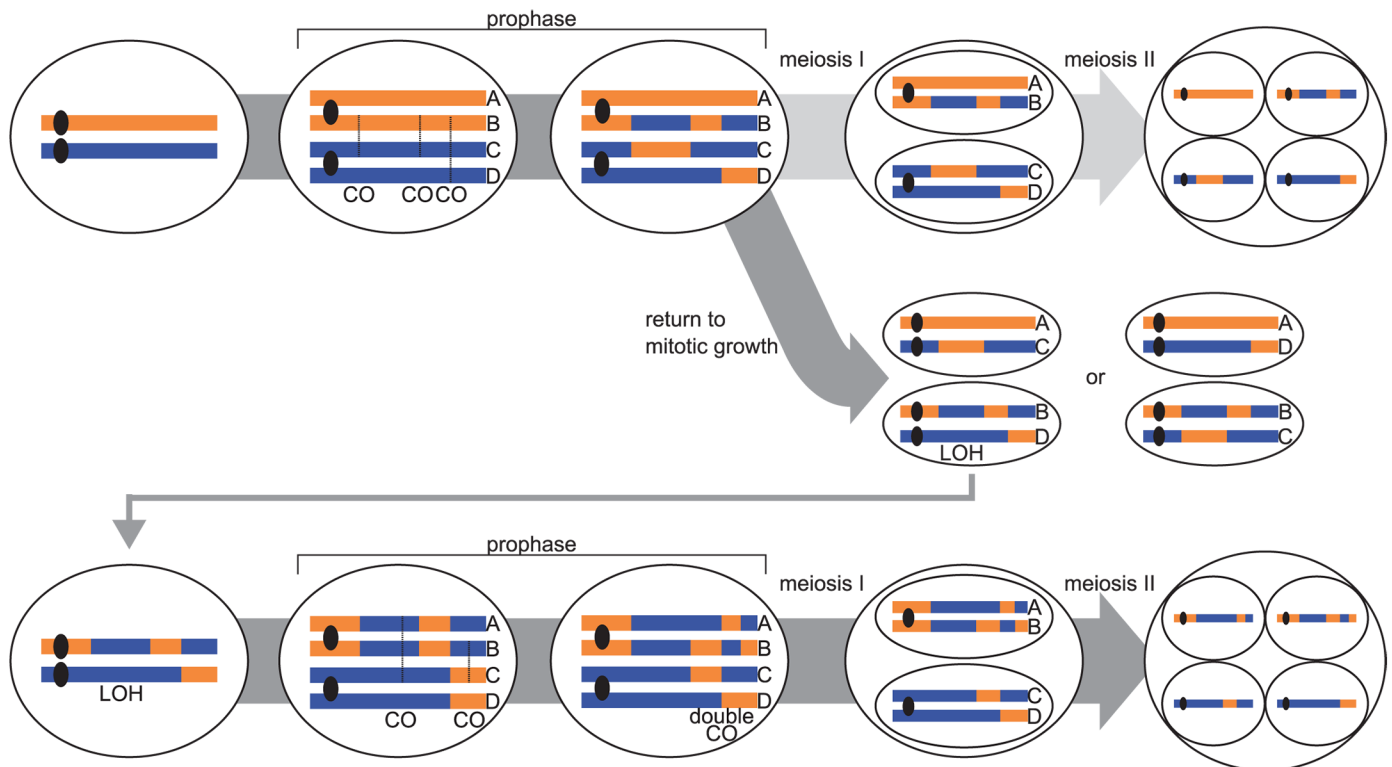
Fig 3. Principle of return to mitotic growth (RTG) after an aborted meiosis followed by a second successful meiosis. After prophase I and inter homolog meiotic recombination, meiosis progression is aborted and chromosomes segregate mitotically by sister chromatid separation only keeping centromeres heterozygous. The resulting diploid cell, if it still has *MAT*a/*MAT*α genotype, can go through a second meiosis. Single COs from the first meiotic prophase are converted into double COs potentially associated with short 4:0 conversion tracts. LOH tracts are converted into large 4:0 segregating tracts. Precise location of COs occurring within LOH tracts cannot be determined.

of *S. cerevisiae* that is rather uncommon in other eukaryotes (Fig 4A). Indeed, the fission yeast *Schizosaccharomyces pombe*, which also harbors a 12.6 Mb genome size, displays a number of COs ranging from 34 to 44 per meiosis, depending on the hybrid studied, leading to approximately 3 COs/Mb per meiosis [34,35]. Recombination analyses were also performed in other more distant fungi species such as *Agaricus bisporus* and *Gibberella zeae*, where the recombination was estimated to be ~0.78 COs/Mb and ~0.65 COs/Mb per meiosis, respectively [36–38].

The size of the smallest chromosome might explain part of the difference in recombination rates [39]. Indeed, species carrying small chromosomes tend to display high recombination rates to stochastically ensure at least one CO on the smallest chromosome. This is illustrated by a negative correlation between the size of the smallest chromosome and the overall recombination rate across species [39]. We compiled meiotic data from 30 species to complete the one obtained in *L. kluyveri* and compared for all of them the recombination rate with the size of the smallest chromosome. As expected, we observed a negative correlation between these two parameters ($R^2 = 0.79$, S9 Fig) and *L. kluyveri* recombination data are consistent with this correlation. Whether the chromosome number, 8 *vs.* 16 in *L. kluyveri* and *S. cerevisiae*, respectively, impacts the global meiotic recombination rate is unknown.

Mechanistically, several hypotheses could explain the reduced rate of COs in *L. kluyveri*, such as less initiating meiotic DSBs than in *S. cerevisiae*, or a more frequent use of the sister chromatid as a template for DSB repair. We therefore compared the DSB level between *S. cerevisiae* and *L. kluyveri* on chromosomes of similar length by pulse-field gel electrophoresis

(PFGE). We performed this experiment in the homozygous diploid CBS10367 isolate that has been independently chosen for its fast and efficient sporulation properties, although it shows a two-hour delay in meiotic entry compared to the *S. cerevisiae* SK1 isolate (S10A Fig). At comparable time points after meiotic induction, *i.e.* four and six hours, respectively, we found similar DSB levels, suggesting that the three to four-fold lower level of recombination in *L. kluyveri* does not come from a corresponding decrease in initiating DSBs (S10B Fig).

The 1-Mb Sakl0C-left region is associated with a low recombination activity

Chromosome C stands as an outlier with significantly less COs per meiosis compared to the other chromosomes (Fig 4A). This specifically comes from the low recombination activity of the 1-Mb left arm of the chromosome C (Sakl0C-left) where no CO was observed and only one NCO in the *PAC10* gene was detected (S6 Fig). *De novo* genome assemblies of the two parental genomes using mate pair sequencing data (see Methods) show that the two chromosomes C are collinear to the chromosome C of the CBS3082 reference strain (S11 Fig). Consequently, the absence of CO on Sakl0C-left is not due to the presence of chromosomal rearrangements such as inversions that could prevent recombination. This low recombination activity of the Sakl0C-left region is unexpected and adds up to the other peculiarities of this genomic region. We recently performed a *L. kluyveri* population genomic survey and showed that this specific region is a relic of an introgression event, which occurred in the last common ancestor [23]. Our study also revealed that the Sakl0C-left region underwent a molecular evolution pattern different from the rest of the genome. It is characterized by a higher GC content, a higher sequence diversity within isolates ($\pi = 0.019$ *vs*. 0.017) as well as a dramatically elevated rate of A:T $\rightarrow$ G:C substitutions. Therefore, the higher density of mutations on Sakl0C-left between our parental strains compared to the rest of the genome (1.13% *vs*. 0.69%) could prevent the use of the homologous chromatid in DSB repair because of the anti-recombination activity of the mismatch repair machinery [24,40]. Another possibility is that fewer DSBs are induced in this region, this being potentially related to the high GC content. To test this latter possibility, we monitored the DSB level on several chromosomes including chromosome C by Southern blot after PFGE of samples from meiotic time courses using the CBS10367 isolate
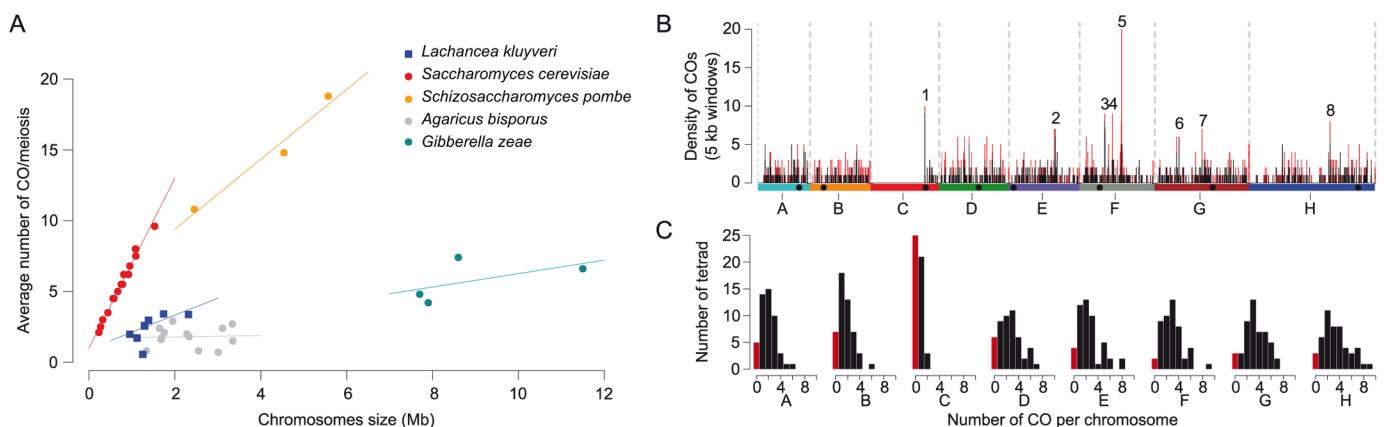
Fig 4. Recombination landscape in *L. kluyveri*. (A) Average number of COs per meiosis per chromosome for five species: Saccharomycontina (*Lk*: intercept = 0.92, slope = 1.2, *Sc*: intercept = 0.99, slope = 6.0), Taphrinomicotina (*Sp*: intercept = 4.5, slope = 2.5), Agaricomycotina (*Ab*: intercept = 1.7, slope = 0.05), Pezizomycotina (*Gz*: intercept = 1.5, slope = 0.47). Data obtained from [34–38]. (B) Density of COs along the genome using a 5 kb window. Regions 1 to 8 correspond to hotspots of COs. Black peaks correspond only to single COs. Red peaks included pre-RTG events (double COs and LOHips). (C) Histogram of the number of COs per meiosis for each *L. kluyveri* chromosome. The red bars correspond to the cases where no CO was detected on the chromosome.
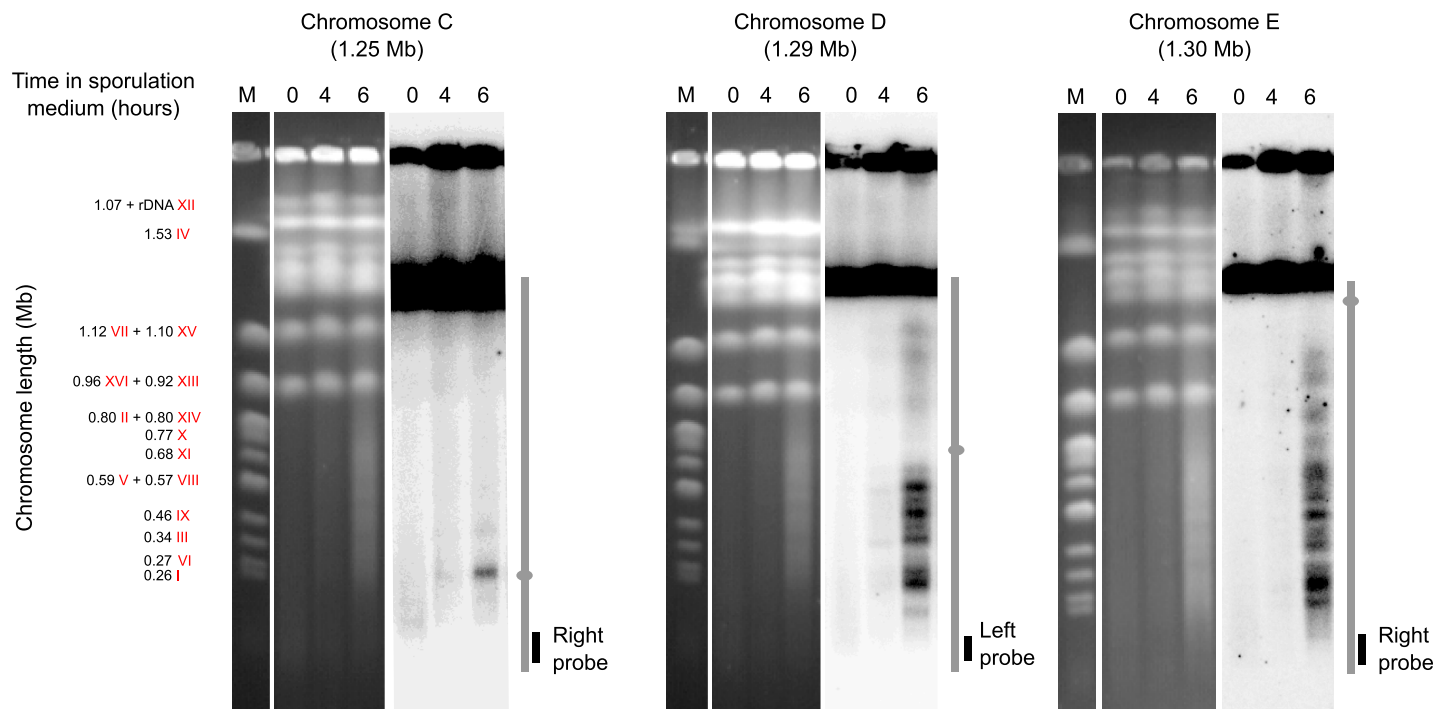
Fig 5. Visualization of meiotic DSB hotspots on *L. kluyveri* chromosomes C, D and E. *L. kluyveri* meiotic chromosomes were separated by PFGE and revealed with telomere proximal probes after Southern blot. The strain CBS10367 *Δsae2/Δsae2* was used for a better visualization of the broken chromosomes. Left parts, ethidium bromide stained gels. Right parts, radioactive signals of the corresponding membranes after Southern blot. M, molecular size marker corresponding to mitotic *S. cerevisiae* chromosomes. Chromosomes are represented vertically, with the location of the probe used. Grey dots indicate centromeres location. Note that the exposure of chromosome C was increased compared to chromosome D and E to better visualize the centromeric proximal DSB hotspot. This underlines the weaker DSB level on chromosome C.

https://doi.org/10.1371/journal.pgen.1006917.g005

(Fig 5). We observed DSB hotspot signals all along chromosomes D and E. Only one centromere proximal hotspot was detected on Sakl0C-left. Finer mapping of this DSB hotspot showed it is located in the promoter region of *GPI18*, matching the CO hotspot number 1 (S12 Fig and see below). This result is remarkable since it reveals a 1Mb region deprived of detectable DSBs. Interestingly, even if the *GPI18* hotspot is located in the Sakl0C-left, it lies close to the centromere outside but flanking the GC rich region. The next unanswered challenge is to determine what makes such a large region refractory to Spo11 cleavage.

Intriguingly, we previously observed that the Sakl0C-left region has an increased ancestral recombination rate estimate ρ (based on linkage disequilibrium decay) compared to the rest of the genome (ρ = 8.5 *vs*. 3.2 Morgans/kb, respectively) [23]. This observation stands in contrast to the actual recombination rate we determined here. An evolution of the recombination rate over time, among other causes, could explain this discrepancy [23,41]. Interestingly, the *MAT* locus is in this region and the unusual absence of recombination revealed here reminds of its suppression associated to the *MAT* locus in fungi species such as *Neurospora tetrasperma* or *Cryptococcus* spp. [42,43], or more generally to sex chromosomes such as the chromosome Y in mammals. The reason of this suppression is unclear but the lack of recombination might result in a long-term degeneration of genes [44].

High incidence of non-recombining chromosomes in *L. kluyveri* tetrads

A consequence of the absence of recombination in the Sakl0C-left is a global deficit of COs on chromosome C (Fig 4A). Strikingly, 25 out of 49 tetrads show no CO on chromosome C but correct chromosome segregation, with four viable spores. In addition, more than half of the

L. kluyveri tetrads on average contained another chromosome without any CO (E0, for 0 exchange) while it happened in only one tetrad out of 46 in *S. cerevisiae* [6] (Fig 4C and S2 Table). Since the presence of E0 chromosomes threatens accurate chromosome segregation at meiosis I, this result suggests either inaccurate chromosome segregation in *L. kluyveri*, notably for chromosome C, and therefore elevated spore death, or the existence of an efficient compensatory mechanism such as distributive segregation [45]. We could not determine the spore viability of the parental strains of our hybrid because no corresponding homozygous diploid was available. However, we determined that the spore viability of the *L. kluyveri* reference strain CBS3082 is close to 100% showing that at least this isolate undergoes proper homolog segregation at meiosis I. Assuming the high frequency of E0 is a general property of this species, this tends to support the existence of an efficient compensatory mechanism for meiotic chromosome segregation in *L. kluyveri*.

CO interference in *L. kluyveri*

By analyzing inter COs distances, we could determine if *L. kluyveri* COs interfere. CO interference is a phenomenon that tends to ensure an even distribution of COs along chromosomes and that may promote efficient chromosome segregation at meiosis I. This feature is not conserved across species as *S. pombe* does not display any CO interference. While the mechanism of CO interference is still unclear, the so-called ZMM group of proteins Zip1, 2, 3, 4, Spo16, Msh4, 5 and Mer3 promote CO interference in *S. cerevisiae* [46]. By contrast to the other *Lachancea* species, *L. kluyveri* conserved all these genes [47], which led us to anticipate the presence of CO interference. We looked for CO interference by measuring inter-CO distances and fitting them to a gamma distribution function characterized by a shape (k, estimating interference) and scale (θ, estimating the inverse of CO rate) parameter [25,48,49]. We first confirmed that *L. kluyveri* displayed CO interference by comparing inter-CO distances distribution to a gamma distribution with no interference (shape parameter (k) = 1, Kolmogorov-Smirnov test P = 0.0072). However, the optimal estimation of the strength of interference in *L. kluyveri* is significantly lower than that of *S. cerevisiae* (k = 1.47 *vs.* 1.96, Kolmogorov-Smirnov test P = 0.015). Additionally, because the COs frequency is low, the scale parameter in *L. kluyveri* is higher than in *S. cerevisiae* (θ = 187 *vs.* 61.7) (S13A Fig). Remarkably, the distribution of size of LOH regions follows approximately the same gamma law (k = 1.45 and θ = 213, S13B Fig), which is in agreement with their meiotic origin.

Recombination hotspots are not conserved between *L. kluyveri* and *S. cerevisiae*

To identify CO hotspots (Fig 4B and S6 Fig), we determined the density of COs along the genome using a 5 kb window, and defined as hotspots the regions displaying seven or more COs per 5 kb ($P < 0.02$ based on 10^5 randomly generated COs positions). In addition to the *VMA1* hotspot discussed previously, seven other CO hotspots were identified across the 49 meioses and 38 RTGs. They are located in the *GPI18*, *RAS1*, *PIS1*, *PRM2*, *OST6*, *VMA10*, and *ALT2* orthologs (hotspot 1, 2, 3, 4, 6, 7, and 8, respectively) (Fig 4B).

As mentioned previously, the *GPI18* CO hotspot is on the left arm of chromosome C at approximately 9 kb from the centromere (hotspot 1, Fig 4B). This corresponds exactly to the end of the 1-Mb introgressed region (Sakl0C-left) and carries relics of transposable elements in both parental strains (S3B Fig). Whether these transposable elements influence DSB formation or not remains to be established, since the presence of such elements is not predictive of the local recombination activity [50]. Another hypothesis is that we enriched the instance of COs happening on the chromosome C by selecting only full viable tetrads, as the absence of

recombination on the Sakl0C-left region might lead to a reduction of the spore viability. In any case, this CO hotspot correlates with the DSB hotspot we observed in the promoter region of *GPI18* from the CBS10367 isolate that also has relics of transposable elements (S12 Fig).

Among the six remaining CO hotspots, four are associated with genes with an expression level above the median during growth in rich medium (S3 Table) [41]. As for *GPI18*, we observed corresponding DSB hotspots in the promoters of *RAS1* (chromosome E) and *PIS1* (chromosome F) (S12 Fig). The comparison of the recombination hotspots between *S. cerevisiae* and *L. kluyveri* is statistically limited by the low recombination rate in the protoploid species. However, none of the well-known recombination hotspots in *S. cerevisiae* were significantly detected in *L. kluyveri* (*e.g. IMG1*, *HIS4*, *CYS3*) [6,8]. In addition, among the eight hotspots detected in *L. kluyveri*, only one is significantly enriched for COs in *S. cerevisiae* considering the meiotic recombination dataset from Mancera *et al.* [6]. We tested the significance of recombination rate difference between the two species in a 10 kb windows (gene-proximal COs) around each pair of orthologs involved in a hotspot of *L. kluyveri*. We confirmed the difference for all the recombination hotspots with the exception of the one located in the syntenic block *MSC7-VMA10-BCD1* (Fisher exact test: $P < 0.01$). At a larger scale, we compared between the two species the number of gene-proximal COs for all pairs of orthologs and observed a poor correlation ($R^2 < 0.01$, Fig 6). The *VMA10* hotspot appears to be the only one conserved between the two species. Interestingly, the *Saccharomyces* species (*e.g. S. cerevisiae*, *Saccharomyces paradoxus*), which are closely related, display similar or conserved recombination patterns, as shown by using population genomics data and comparing genome-wide recombination initiation maps [15,17]. We investigated a potential link between the location of the recombination events and different local properties of the genome such as GC content, gene density and marker density. No significant correlation was found. However, this might be partially due to the small number of meiotic events analyzed (S3 Fig). Here, our results demonstrate that the distribution of meiotic recombination is not persistent across distantly related yeast species covering a large evolutionary scale, exceeding the one of the *Saccharomyces* genus. A possible factor explaining the conservation of repartition of recombination across this genus is the shared synteny and chromosomal organization.

Conclusion

Genome evolution is strongly tied to the meiotic behavior and recombination landscape. With the exploration of the meiotic genetic exchanges of a protoploid yeast species and its comparison to *S. cerevisiae* as well as other fungi (Fig 4A), we unveiled characteristics that brought a new light on the variation of the recombination landscape and its potential impact on evolution. The lack of recombination hotspot conservation between *L. kluyveri* and *S. cerevisiae* might result from synteny breakage that would modify the cis interactions between recombination hotspots previously distant from one another. Short- and long-range cis interactions between recombination initiation sites have been previously observed and discussed in *S. cerevisiae* [51]. They include short-range competition for DSB factors [52] and Tel1-mediated DSB interference in cis over distances spanning several meiotic chromatin loops [53]. Our data could therefore support a direct link between synteny breakage on recombination hotspots evolution. However, we cannot exclude that recombination hotspots also evolve independently of synteny breakage in yeast as in *Drosophila* that do not have PRDM9 like elements [54], but that would be at a much slower speed since recombination initiation hotspots are conserved over the entire *Saccharomyces* clade. Exploration of the recombination landscape across a larger number of yeast species spanning a broad evolutionary distance will be important to understand better the effect of synteny breakage on recombination hotspots evolution.
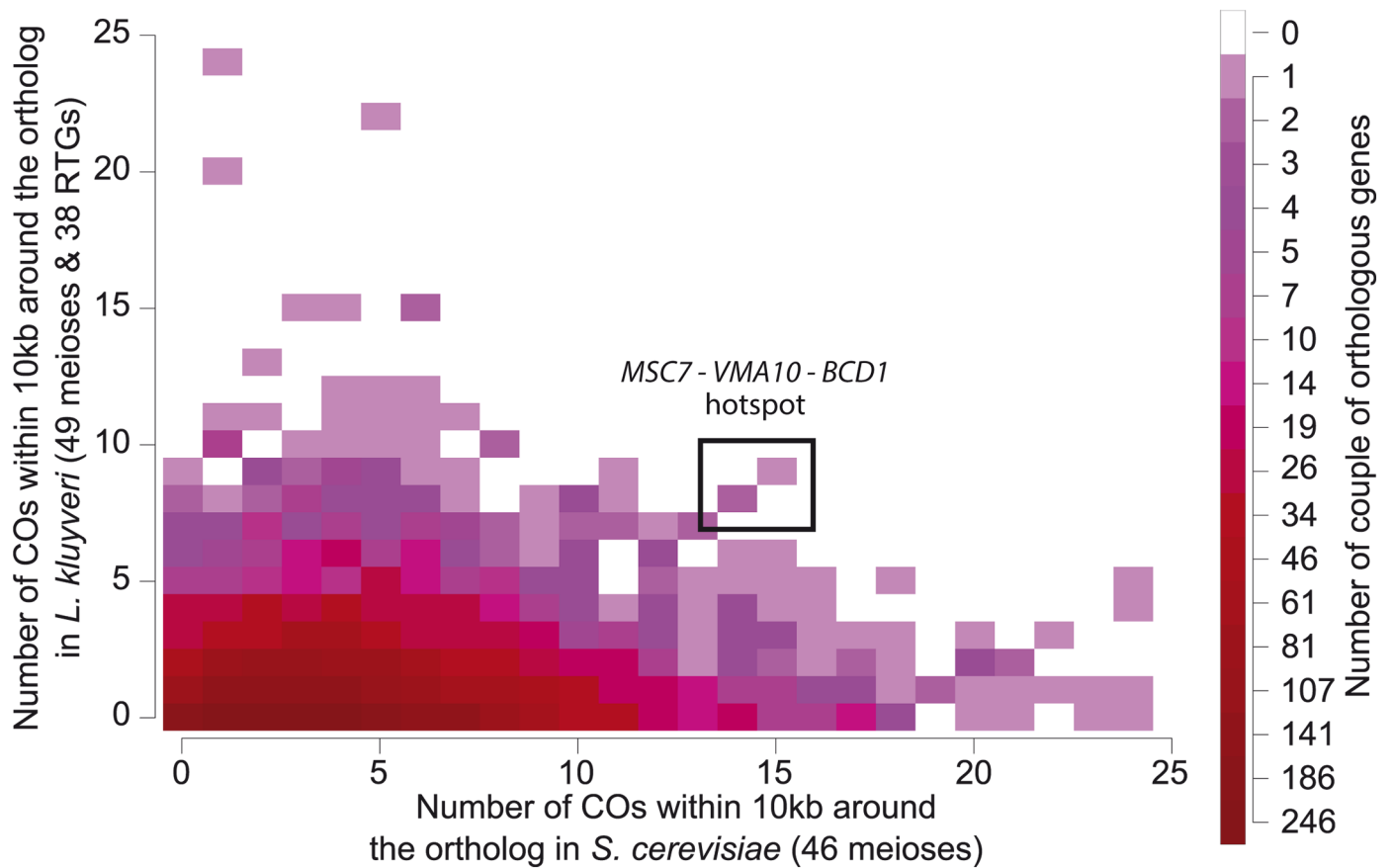
Fig 6. Comparison of the number of proximal COs between *S. cerevisiae* and *L. kluyveri* orthologs. For each ortholog pair, we determined the number of COs in a 10kb window around each gene. The plot displays the density of ortholog pairs according to the associated number of proximal COs. The conservation of COs position between species would generate a linear correlation, with several instances located in the upper-right part of the plot. Here, the R^2 of the linear regression is 1.16×10^{-3} ($P = 8.22 \times 10^{-3}$). The unique common hotspot between the two species is *MSC7-VMA10-BCD1*.

A striking feature of *L. kluyveri* is the almost complete absence of recombination in a 1-Mb region of the chromosome C, resulting in the absence of CO on this whole chromosome for about half of the analyzed tetrads. We showed that this results from a lack of Spo11-induced DSB in the corresponding region. What prevents Spo11 from making DSBs over such a long region and the consequences of this meiotic defect remain to be determined. Interestingly, the absence of recombination in this introgressed region that determines mating-types has the consequence to genetically link all the genes and therefore all phenotypic characteristics their alleles might induce, which potentially hindered species diversification and adaptation.

The capacity for *L. kluyveri* hybrids to undergo RTG during stress, resulting in a high number of LOH regions, is an unexpected source of genetic and therefore phenotypic diversity. Meiotic reversions are generally not taken into account in the exploration of species evolution. They have been mainly described in *S. cerevisiae* and little is known about their occurrence across any other yeast species. Moreover, it is difficult to estimate the frequency of meiotic reversions in natural conditions. For instance, LOHs detected in natural isolates could be the results of mitotic recombination or inbreeding. Here, our data show that the control of commitment into meiosis might be weaker in some yeast species, increasing allelic shuffling during

stress. The significance of this evolutive advantage needs to be further investigated as it has been underestimated so far.

Our unexpected observations obtained by the deep exploration of recombination landscape of a non-conventional yeast species also demonstrate that yet many mechanisms and variations affecting evolution still remain to be described and explored.

Materials and methods

Strains construction, growth conditions and tetrad dissection

Both parental strains NBRC10955a (*MAT*a) and 67–588 (*MAT*α) had their *CHS3* gene encoding for chitin synthase inactivated to facilitate tetrad dissection [23,55]. Cells were electroporated with a DNA fragment containing the drug resistance marker *KanMX*, produced by fusion PCR [29]. Gene replacement was validated by PCR. All primers are listed in S4 Table.

Growth and cross were performed on YPD (yeast extract 1%, peptone 2%, glucose 2%) at 30˚C. Sporulation was induced by plating cells on sporulation medium (agar 2%, potassium acetate 1%) and incubating 2 to 7 days at 30˚C. The asci of the tetrads were digested using zymolyase (0.5 mg/mL MP Biomedicals MT ImmunO 20T) and the spores were isolated using the MSM 400 dissection microscope (Singer instrument). The whole genome of each of the 196 spores from the 49 full viable tetrads selected was sequenced.

Genomic DNA extraction, sequencing, SNP calling and data analysis

Genomic DNA was extracted using the MasterPure Yeast DNA Purification Kit (tebu-bio) and sequenced using Illumina HiSeq 2000 technology. We used paired-end libraries and 100 bp per read. The average reads coverage is 204x and 100x for NBRC10955a and 67–588, respectively, and around 70x for each of the 196 spores. The reads obtained were cleaned, trimmed and aligned to the reference genome using BWA (-n 8 -o 2 option). Raw data are available on the European Nucleotide Archive (http://www.ebi.ac.uk/ena) under accession number PRJEB13706.

To select SNPs to be used as genotyping markers, the reads of the parental strains NBRC 10955a and 67–588 were mapped against the reference genome, in which repetitive and transposable elements were masked with RepeatMasker. SAMtools was used to call variants, and a set of high quality differential SNPs between parental strains was generated. To be integrated in this set, differential positions must be, for both parents, (I) covered between 50x and 300x, (ii) have a mapping quality score higher or equal to 100, (iii) have an associated allele frequency (AF tag in VCF file) of 0 or 1, and (iv) should not be located in close proximity (10 base pairs) to an indel (insertion/deletion). The final set consists of 58,256 markers used to genotype the progeny.

The reads associated with each spore were mapped and variants called with the same strategy as for the parental strains. At each position of the set, a parental origin was assigned if the residue (i) corresponds to one parental version, (ii) shows a coverage higher than 25% of the average coverage of the spore (20x in most cases), (iii) has a mapping quality higher than 100, and (iv) displays an allele frequency of 0 or 1. If not, a NA flag was assigned to the position.

From this matrix (58,256 × 196 genotypes), we discarded markers flagged NA across 60 spores (30%) or more, markers displaying unbalanced genotype origin in the population (fraction of parental origins above 70% / under 30%) as well as subtelomeric regions carrying translocated and duplicated regions. Finally 56,612 markers corresponding to high quality differential SNPs between parents and for which most of the spores displayed a reliable allelic origin were used. The matrix of genotypes is available (see Supplementary data).

Identification of recombination events

To identify the localization and size of recombination events, including GCs with or without COs and LOH, we adapted the CrossOver python scripts from the Recombine pipeline (http://sourceforge.net/projects/recombine/) [25] to fit *L. kluyveri* genomic characteristics. For each tetrad, we disregarded markers for which at least one spore displayed a NA flag before running CrossOver. In order to conserve only reliable information, a GC event was considered only when at least three markers were involved, which corresponds to 63% of the detected GCs. We defined a LOH as a 4:0 GC event larger than 10 kb (Fig 1). LOH regions detected were validated in one tetrad by looking at the sequence data directly. To do so, pooled reads of all four spores from the selected tetrad were aligned to the reference genome (BWA), and the polymorphic positions were identified (SAMtools). Regions without LOH would present both parental allelic versions and thus appear to be heterozygous, whereas LOH regions would be homozygous. The detected homozygous regions coincide with LOH regions identified using CrossOver (S4 Fig). All detected meiotic recombination events are provided in S5 Table and a global summary of the number of events detected per chromosome and per tetrad in S2 Table.

The number of COs occurring within LOH regions was estimated based on the recombination rate. A total of 875 COs has been detected in the genomes of 49 meioses, excluding the Sakl0C-left region and LOH regions (416.4 Mb). The cumulative size of all the LOH regions was 90.4 Mb. With the hypothesis that the recombination rate is homogeneous, we estimated that 190 COs occurred within LOH regions of our meiotic sample.

Not all of the recombination events occurring during RTG can be observed in the final tetrad as only two of the four RTG chromatids are conserved (Fig 3). A previous study estimated that the underestimation of the RTG is about 2/3 but it depends on the recombination rate as well as the chromosome size [31].

Quantification of meiotic DSBs

S. cerevisiae SK1 [53] and *L. kluyveri* CBS10367 [23] diploid strains homozygous for the *sae2* null allele were used to detect the level of cut chromosomes during meiotic time courses. Procedures relative to *S. cerevisae*, Southern blot analysis and chromosome preparation in agarose plugs are as described in [53]. Oligonucleotide sequences for probe synthesis are in S4 Table. *L. kluyveri* cells were inoculated in pre-sporulation medium (0.5% yeast extract, 1% peptone, 0.17% yeast nitrogen base, 1% potassium acetate, 1% ammonium sulfate, 0.5% potassium phthalate, pH 5.5) over night at 30˚C to reach an OD_{600} of 1, washed once with water and resuspended in 1% potassium acetate at 30˚C. Cells were harvested at different time points, washed with water and frozen. Pulse field gel electrophoreses were performed using a Bio Rad CHEF DRIII apparatus at 14˚C, initial switch time 60 seconds, final switch time 120 seconds, 6 V/cm, angle 120˚ for 20h.

de novo assembly of the parental genomes

SOAPdenovo (v2.04, [56]) was used to construct *de novo* assemblies for both parental strains using a combination of paired-end and mate-pair Illumina reads (European Nucleotide Archive: PRJEB13706). We tested a range of k-mer size (from 45 to 83) and compared the obtained assemblies at the contiguity level. We found k = 63 and k = 71 to be optimal for the 67–588 and NBRC10955 parental strains, respectively. The selected assemblies were compared to the reference genome with nucmer [57] and results were plotted with mummerplot (S11 Fig).

Supporting information

S1 Fig. Spore viability of the NBRC10955 × 67–588 progeny. A total of 120 tetrads were dissected. Among the full tetrads, 49 were selected for genotyping.
(EPS)

S2 Fig. Genetic map based on 56,612 SNPs segregating between the two parental strains.
(EPS)

S3 Fig. Comparison of the recombination, gene density, GC content and marker density landscapes. (A) Profiles of the 8 chromosomes. Densities were calculated using a 20-kb sliding window. Dots indicate the number of COs and NCOs per 10-kb. *L. kluyveri* have point centromeres similar to the *Saccharomyces* species. (B) Zoom on the chromosome C recombination hotspots. The blue lines indicate the positions of the regions of gene conversion associated to the 9 COs detected. The GC content is calculated for each of the open reading frames.
(EPS)

S4 Fig. Identification of subtelomeric translocations and duplications. These regions were identified based on marker genetic linkage across spores, heterozygosity level and read coverage. The low quality regions contain markers displaying noisy signals and incoherent segregations. All these regions were disregarded in the analysis of recombination. All markers between the telomere and the case-by-case cut-off position were excluded.
(EPS)

S5 Fig. LOH events during mitosis and within a tetrad. (A) Position and allele balance of heterozygous sites from the initial parental diploid. (B) Position and allele balance of heterozygous sites in two evolved parental diploids after accumulation of mitoses. The heterozygous sites cover the totality of the genome in all cases, indicating the absence of LOH formation during mitosis. (C) Position and allele balance of heterozygous sites identified using the fusion of the reads of the four spores of tetrad 1. Regions with no heterozygous sites correspond to LOH events. (D) Position along the genome of the LOH identified in the tetrad 1 using CrossOver program [25]. These regions overlap with those detected using heterozygous sites.
(EPS)

S6 Fig. Genomic localization of all meiotic recombination events from 49 meioses. Pink region corresponds to the Sakl0C-left introgressed region, which is a recombination coldspot. Regions 1 to 8 correspond to meiotic recombination hotspots. The density is provided using a 5 kb window.
(EPS)

S7 Fig. Vma1-derived PI-Sce1 endonuclease homing mechanism and its repartition within the collection of sequenced *L. kluyveri* isolates. (A) The PI-Sce1 location within *VMA1* is given in nucleotides. During meiosis, PI-Sce1 protein self-spliced from the Vma1 protein targets a short DNA sequence of ~ 20 base pairs present in an empty *VMA1* gene and induces a DNA double strand break [32]. The recombinational repair using the homolog transfers the PI-Sce1 sequence in the initially empty *VMA1* gene, with or without associated CO. (B) PI-Sce1 repartition in the panel of 28 sequenced isolates displayed on a neighbor-joining tree based polymorphic sites [23].
(EPS)

S8 Fig. RTG and meiotic recombination rates. Frequency of recombination (A: pre-RTG; B: final meiosis). Average numbers of COs events detected are 16 and 19.9 per RTG and meiosis, respectively. Pre-RTG are under-estimated since not all events are conserved in the

transitional diploid [31].
(EPS)

S9 Fig. Correlation between the smallest chromosome length and the average recombination rate. Data across 31 species were obtained from Mercier et al. 2014 [35]. Linear regression: $R^2 = 0.79$, $P < 10–7$.
(EPS)

S10 Fig. *L. kluyveri* and *S. cerevisiae* show similar levels of DSBs at comparable time points. (A) *L. kluyveri* CBS10367 and *S. cerevisiae* SK1 meiotic progression determined by counting cells which went through meiotic I or II stages after DAPI staining. Errors bars indicate standard deviations from three independent cultures. At least 100 cells per culture were counted. *S. cerevisiae* cultures enter meiosis around two hours before *L. kluyveri* cultures. (B) Wild type *L. kluyveri* CBS10367 and *S. cerevisiae* SK1 meiotic chromosomes were separated by PFGE and revealed by telomere proximal probes after Southern blot. The peak of DSB in WT conditions occurs at 4h in *S. cerevisiae* and 6h in *L. kluyveri*. Quantification of the corresponding signals show similar DSB levels between the two strains (black rectangles). Cut / uncut represents the cumulated signals from all the cut fragments divided by the signal from all fragments (full length and cut chromosome as well as the signal from the well). Quantifications were made from three independent experiments and error bars show standard deviations. (C) Same as in B except that a *Δsae2/Δsae2* background was used to stabilize broken chromosomes as illustrated by the stronger cut signals with respect to the wild type background.
(EPS)

S11 Fig. Alignment of the de novo parental genome assemblies from 67–588 (A) and NBRC 10955 (B) with the reference CBS 3082 genome. Assemblies were constructed with SOAPdenovo using a combination of paired-end and mate-pair Illumina reads. Chromosome C from the three species show no rearrangement and are completely collinear.
(EPS)

S12 Fig. Visualization of individual meiotic DSB hotspots at three loci. *L. kluyveri* meiotic DNA was digested by PflMI (*GPI18* and *PIS1* loci) and BsaI (*RAS1* locus), separated by standard gel electrophoresis and revealed with locus specific probes after Southern blot. The strain CBS10367 *Δsae2/Δsae2* was used. Left parts, ethidium bromide stained gels showing the corresponding DNA ladder (M). Right parts, radioactive signals after Southern blot. Genomic loci are schematized on the right. Arrows represent ORFs with their corresponding orientations. Vertical black bars represent the probes used. The stars indicate the DSB hotspot locations. *GPI18*, *RAS1* and *PIS1* loci correspond to recombination hotspots 1, 2, 3 from chromosomes C, E, F, respectively.
(EPS)

S13 Fig. Interference between COs. (A) Inter-CO distances histogram. Parameters of gamma distribution modeled from these data (red line) were estimated: shape k = 1.47 and scale θ = 187. This distribution is compared to the one detected in S. cerevisiae (blue dotted line): shape k = 1.96 and scale θ = 61.7 [25]. (B) LOH size histogram. Parameters of gamma distribution modeled from these data (red line) were estimated: shape k = 1.45 and scale θ = 213.
(EPS)

S1 Table. Detail of calculation for each type of recombination event detected.
(XLSX)

S2 Table. Summary of meiotic events detected by tetrad and by chromosome.
(XLSX)

S3 Table. List of the genes at the proximity of crossover hotspots.
(XLSX)

S4 Table. Oligonucleotides for the deletion of *CHS3* and Southern blot probes.
(XLSX)

S5 Table. List of the meiotic events detected within the 49 disected tetrads.
(XLSX)

S1 Data. Genotyping data of all the *Lachancea kluyveri* segregants.
(GZ)

Acknowledgments

Author Contributions

References

1. Petronczki M, Siomos MF, Nasmyth K. Un ménage à quatre: the molecular biology of chromosome segregation in meiosis. Cell. 2003; 112: 423–440. PMID: 12600308

2. Haber JE. Evolution of models of homologous recombination. Recombination and meiosis. Springer Berlin Heidelberg; 2007. pp. 1–64.

3. Keeney S, Giroux CN, Kleckner N. Meiosis-specific DNA double-strand breaks are catalyzed by Spo11, a member of a widely conserved protein family. Cell. 1997; 88: 375–384. PMID: 9039264

4. Pan J, Sasaki M, Kniewel R, Murakami H, Blitzblau HG, Tischfield SE, et al. A hierarchical combination of factors shapes the genome-wide topography of yeast meiotic recombination initiation. Cell. 2011; 144: 719–731. https://doi.org/10.1016/j.cell.2011.02.009 PMID: 21376234

5. Zickler D, Kleckner N. Meiotic chromosomes: integrating structure and function. Annu Rev Genet. 1999; 33: 603–754. https://doi.org/10.1146/annurev.genet.33.1.603 PMID: 10690419

6. Mancera E, Bourgon R, Brozzi A, Huber W, Steinmetz LM. High-resolution mapping of meiotic crossovers and non-crossovers in yeast. Nature. 2008; 454: 479–485. https://doi.org/10.1038/nature07135 PMID: 18615017

7.   Gerton JL, DeRisi J, Shroff R, Lichten M, Brown PO, Petes TD. Global mapping of meiotic recombination hotspots and coldspots in the yeast Saccharomyces cerevisiae. Proc Natl Acad Sci U S A. 2000; 97: 11383–11390. https://doi.org/10.1073/pnas.97.21.11383 PMID: 11027339

8.   Lichten M, Goldman AS. Meiotic recombination hotspots. Annu Rev Genet. 1995; 29: 423–444. https://doi.org/10.1146/annurev.ge.29.120195.002231 PMID: 8825482

9.   Hultén MA. On the origin of crossover interference: A chromosome oscillatory movement (COM) model. Mol Cytogenet. 2011; 4: 10. https://doi.org/10.1186/1755-8166-4-10 PMID: 21477316

10. Wang S, Zickler D, Kleckner N, Zhang L. Meiotic crossover patterns: obligatory crossover, interference and homeostasis in a single process. Cell Cycle Georget Tex. 2015; 14: 305–314.

11. Zickler D, Kleckner N. A few of our favorite things: Pairing, the bouquet, crossover interference and evolution of meiosis. Semin Cell Dev Biol. 2016; 54: 135–148. https://doi.org/10.1016/j.semcdb.2016.02.024 PMID: 26927691

12. Boulton A, Myers RS, Redfield RJ. The hotspot conversion paradox and the evolution of meiotic recombination. Proc Natl Acad Sci U S A. 1997; 94: 8058–8063. PMID: 9223314

13. Berg IL, Neumann R, Lam K-WG, Sarbajna S, Odenthal-Hesse L, May CA, et al. PRDM9 variation strongly influences recombination hot-spot activity and meiotic instability in humans. Nat Genet. 2010; 42: 859–863. https://doi.org/10.1038/ng.658 PMID: 20818382

14. Coop G, Wen X, Ober C, Pritchard JK, Przeworski M. High-resolution mapping of crossovers reveals extensive variation in fine-scale recombination patterns among humans. Science. 2008; 319: 1395–1398. https://doi.org/10.1126/science.1151851 PMID: 18239090

15. Lam I, Keeney S. Nonparadoxical evolutionary stability of the recombination initiation landscape in yeast. Science. 2015; 350: 932–937. https://doi.org/10.1126/science.aad0814 PMID: 26586758

16. Ptak SE, Hinds DA, Koehler K, Nickel B, Patil N, Ballinger DG, et al. Fine-scale recombination patterns differ between chimpanzees and humans. Nat Genet. 2005; 37: 429–434. https://doi.org/10.1038/ng1529 PMID: 15723063

17. Tsai IJ, Burt A, Koufopanou V. Conservation of recombination hotspots in yeast. Proc Natl Acad Sci U S A. 2010; 107: 7847–7852. https://doi.org/10.1073/pnas.0908774107 PMID: 20385822

18. Zanders SE, Eickbush MT, Yu JS, Kang J-W, Fowler KR, Smith GR, et al. Genome rearrangements and pervasive meiotic drive cause hybrid infertility in fission yeast. eLife. 2014; 3.

19. Singhal S, Leffler EM, Sannareddy K, Turner I, Venn O, Hooper DM, et al. Stable recombination hotspots in birds. Science. 2015; 350: 928–932. https://doi.org/10.1126/science.aad0843 PMID: 26586757

20. Dujon B. Yeasts illustrate the molecular mechanisms of eukaryotic genome evolution. Trends Genet. 2006; 22: 375–387. https://doi.org/10.1016/j.tig.2006.05.007 PMID: 16730849

21. Kellis M, Birren BW, Lander ES. Proof and evolutionary analysis of ancient genome duplication in the yeast Saccharomyces cerevisiae. Nature. 2004; 428: 617–624. https://doi.org/10.1038/nature02424 PMID: 15004568

22. Wolfe KH, Shields DC. Molecular evidence for an ancient duplication of the entire yeast genome. Nature. 1997; 387: 708–713. https://doi.org/10.1038/42711 PMID: 9192896

23. Friedrich A, Jung P, Reisser C, Fischer G, Schacherer J. Population genomics reveals chromosome-scale heterogeneous evolution in a protoploid yeast. Mol Biol Evol. 2015; 32: 184–192. https://doi.org/10.1093/molbev/msu295 PMID: 25349286

24. Martini E, Borde V, Legendre M, Audic S, Regnault B, Soubigou G, et al. Genome-wide analysis of heteroduplex DNA in mismatch repair-deficient yeast cells reveals novel properties of meiotic recombination pathways. PLoS Genet. 2011; 7: e1002305. https://doi.org/10.1371/journal.pgen.1002305 PMID: 21980306

25. Anderson CM, Chen SY, Dimon MT, Oke A, DeRisi JL, Fung JC. ReCombine: a suite of programs for detection and analysis of meiotic recombination in whole-genome datasets. PloS One. 2011; 6: e25509. https://doi.org/10.1371/journal.pone.0025509 PMID: 22046241

26. Sherman F, Roman H. Evidence for two types of allelic recombination in yeast. Genetics. 1963; 48: 255–261. PMID: 13977170

27. Simchen G. Commitment to meiosis: what determines the mode of division in budding yeast? BioEssays News Rev Mol Cell Dev Biol. 2009; 31: 169–177.

28. Tsuchiya D, Yang Y, Lacefield S. Positive Feedback of NDT80 Expression Ensures Irreversible Meiotic Commitment in Budding Yeast. PLOS Genet. 2014; 10: e1004398. https://doi.org/10.1371/journal.pgen.1004398 PMID: 24901499

29. Brion C, Pflieger D, Souali-Crespo S, Friedrich A, Schacherer J. Differences in environmental stress response among yeasts is consistent with species-specific lifestyles. Mol Biol Cell. 2016; 27: 1694–1705. https://doi.org/10.1091/mbc.E15-12-0816 PMID: 27009200

30. Hagman A, Säll T, Compagno C, Piskur J. Yeast "make-accumulate-consume" life strategy evolved as a multi-step process that predates the whole genome duplication. PLoS One. 2013; 8(7):e68734. https://doi.org/10.1371/journal.pone.0068734 PMID: 23869229

31. Laureau R, Loeillet S, Salinas F, Bergström A, Legoix-Né P, Liti G, et al. Extensive recombination of a yeast diploid hybrid through meiotic reversion. PLoS Genet. 2016; 12: e1005781. https://doi.org/10.1371/journal.pgen.1005781 PMID: 26828862

32. Gimble FS, Thorner J. Homing of a DNA endonuclease gene by meiotic gene conversion in *Saccharomyces cerevisiae*. Nature. 1992; 357: 301–306. https://doi.org/10.1038/357301a0 PMID: 1534148

33. Okuda Y, Sasaki D, Nogami S, Kaneko Y, Ohya Y, Anraku Y. Occurrence, horizontal transfer and degeneration of VDE intein family in Saccharomycete yeasts. Yeast Chichester Engl. 2003; 20: 563–573.

34. Clément-Ziza M, Marsellach FX, Codlin S, Papadakis MA, Reinhardt S, Rodríguez-López M, et al. Natural genetic variation impacts expression levels of coding, non-coding, and antisense transcripts in fission yeast. Mol Syst Biol. 2014; 10.

35. Mercier R, Mézard C, Jenczewski E, Macaisne N, Grelon M. The molecular biology of meiosis in plants. Annu Rev Plant Biol. 2015; 66: 297–327. https://doi.org/10.1146/annurev-arplant-050213-035923 PMID: 25494464

36. Foulongne-Oriol M, Dufourcq R, Spataro C, Devesse C, Broly A, Rodier A, et al. Comparative linkage mapping in the white button mushroom *Agaricus bisporus* provides foundation for breeding management. Curr Genet. 2011; 57: 39–50. https://doi.org/10.1007/s00294-010-0325-z PMID: 21046108

37. Lee J, Jurgenson JE, Leslie JF, Bowden RL. Alignment of genetic and physical maps of Gibberella zeae. Appl Environ Microbiol. 2008; 74: 2349–2359. https://doi.org/10.1128/AEM.01866-07 PMID: 18263740

38. Morin E, Kohler A, Baker AR, Foulongne-Oriol M, Lombard V, Nagy LG, et al. Genome sequence of the button mushroom *Agaricus bisporus* reveals mechanisms governing adaptation to a humic-rich ecological niche. Proc Natl Acad Sci U S A. 2012; 109: 17501–17506. https://doi.org/10.1073/pnas.1206847109 PMID: 23045686

39. Li W, Freudenberg J. Two-parameter characterization of chromosome-scale recombination rate. Genome Res. 2009; 19: 2300–2307. https://doi.org/10.1101/gr.092676.109 PMID: 19752285

40. Hunter N, Chambers SR, Louis EJ, Borts RH. The mismatch repair system contributes to meiotic sterility in an interspecific yeast hybrid. EMBO J. 1996; 15: 1726–1733. PMID: 8612597

41. Brion C, Pflieger D, Friedrich A, Schacherer J. Evolution of intraspecific transcriptomic landscapes in yeasts. Nucleic Acids Res. 2015; 43: 4558–4568. https://doi.org/10.1093/nar/gkv363 PMID: 25897111

42. Idnurm A, Hood ME, Johannesson H, Giraud T. Contrasted patterns in mating-type chromosomes in fungi: hotspots versus coldspots of recombination. Fungal Biol Rev. 2015; 29: 220–229. https://doi.org/10.1016/j.fbr.2015.06.001 PMID: 26688691

43. Menkis A, Jacobson DJ, Gustafsson T, Johannesson H. The mating-type chromosome in the filamentous ascomycete *Neurospora tetrasperma* represents a model for early evolution of sex chromosomes. PLoS Genet. 2008; 4: e1000030. https://doi.org/10.1371/journal.pgen.1000030 PMID: 18369449

44. Charlesworth B, Charlesworth D. The degeneration of Y chromosomes. Philos Trans R Soc Lond B Biol Sci. 2000; 355: 1563–1572. https://doi.org/10.1098/rstb.2000.0717 PMID: 11127901

45. Guacci V, Kaback DB. Distributive disjunction of authentic chromosomes in *Saccharomyces cerevisiae*. Genetics. 1991; 127: 475–488. PMID: 2016050

46. Lynn A, Soucek R, Börner GV. ZMM proteins during meiosis: crossover artists at work. Chromosome Res Int J Mol Supramol Evol Asp Chromosome Biol. 2007; 15: 591–605.

47. Vakirlis N, Sarilar V, Drillon G, Fleiss A, Agier N, Meyniel J-P, et al. Reconstruction of ancestral chromosome architecture and gene repertoire reveals principles of genome evolution in a model yeast genus. Genome Res. 2016; 26: 918–932. https://doi.org/10.1101/gr.204420.116 PMID: 27247244

48. McPeek MS, Speed TP. Modeling interference in genetic recombination. Genetics. 1995; 139: 1031–1044. PMID: 7713406

49. Zhao H, Speed TP, McPeek MS. Statistical analysis of crossover interference using the chi-square model. Genetics. 1995; 139: 1045–1056. PMID: 7713407

50. Sasaki M, Tischfield SE, van Overbeek M, Keeney S. Meiotic recombination initiation in and around retrotransposable elements in *Saccharomyces cerevisiae*. PLoS Genet. 2013; 9: e1003732. https://doi.org/10.1371/journal.pgen.1003732 PMID: 24009525

51. Robine N, Uematsu N, Amiot F, Gidrol X, Barillot E, Nicolas A, Borde V. Genome-wide redistribution of meiotic double-strand breaks in *Saccharomyces cerevisiae*. Mol Cell Biol. 2007; 27(5):1868–80. https://doi.org/10.1128/MCB.02063-06 PMID: 17189430

52. Wu TC, Lichten M. Factors that affect the location and frequency of meiosis-induced double-strand breaks in *Saccharomyces cerevisiae*. Genetics. 1995; 140(1):55–66. PMID: 7635308

53. Garcia V, Gray S, Allison RM, Cooper TJ, Neale MJ. Tel1(ATM)-mediated interference suppresses clustered meiotic double-strand-break formation. Nature. 2015; 520: 114–118. https://doi.org/10.1038/nature13993 PMID: 25539084

54. Comeron JM, Ratnappan R, Bailin S. The many landscapes of recombination in *Drosophila melanogaster*. PLoS Genet. 2012; 8(10):e1002905 https://doi.org/10.1371/journal.pgen.1002905 PMID: 23071443

55. Sigwalt A, Caradec C, Brion C, Hou J, de Montigny J, Jung P, et al. Dissection of quantitative traits by bulk segregant mapping in a protoploid yeast species. FEMS Yeast Res. 2016; pii: fow056.

56. Luo R, Liu B, Xie Y, Li Z, Huang W, Yuan J, et al. SOAPdenovo2: an empirically improved memory-efficient short-read *de novo* assembler. GigaScience. 2012; 1: 18. https://doi.org/10.1186/2047-217X-1-18 PMID: 23587118

57. Delcher AL, Phillippy A, Carlton J, Salzberg SL. Fast algorithms for large-scale genome alignment and comparison. Nucleic Acids Res. 2002; 30: 2478–2483. PMID: 12034836